RSC Advances

PAPER

View Article Online
View Journal | View Issue

Cite this: *RSC Adv.*, 2021, **11**, 35567

Giant spin pumping at the ferromagnet (permalloy) – organic semiconductor (perylene diimide) interface†

Talluri Manoj,[a] Srinu Kotha,[b] Bibekananda Paikaray,[a] Dasari Srideep,[b] Arabinda Haldar,[c] Kotagiri Venkata Rao*[b] and Chandrasekhar Murapaka*[a]

Received 2nd October 2021
Accepted 21st October 2021

DOI: 10.1039/d1ra07349d

rsc.li/rsc-advances

Pure spin current based devices have attracted great interest in recent days. Spin current injection into non-magnetic materials is essential for the design and development of such pure spin current based devices. In this context, organic semiconductors (OSCs) can be potential non-magnetic materials over widely explored heavy metals. This is due to the relatively low spin–orbit coupling of OSCs, which is essential to host the spin current with a large spin diffusion length and long spin-relaxation time. This research work demonstrates the harvesting of spin currents at the perylene diimide (PDI)/permalloy (Py) based OSC interface. The observed high linewidth broadening of 2.18 mT from the ferromagnetic resonance spectra indicates the presence of giant spin pumping from Py to PDI. The resultant spin-mixing conductance, 1.54×10^{18} m^{-2} quantifies the amount of spin current injected from Py to PDI, which is in a similar range to ferromagnet/heavy metals.

Introduction

Spintronics holds great promise for potentially replacing charge based microelectronic technology due to its attractive features of non-volatility, low power consumption, high speed and radiation hardness.[1–4] Spintronic devices work based on the manipulation of the spin property of the electron along with its charge for information storage, processing and transmission. Recent advances in the spintronic community are focused on the generation, manipulation and detection of pure spin currents. The key advantage of pure spin current based devices is the absence of net flow of charge but a transfer of spin angular momentum.[5–7] One of the prominent techniques developed for the generation of pure spin current is the spin pumping method where the spin current is injected from a ferromagnetic (FM) material to an adjacent non-magnetic (NM) material. This process involves the excitation of magnetization precession in the FM under ferromagnetic resonance (FMR) conditions where the large precession of the magnetization leads to angular momentum transfer at the FM/NM interface.[8,9] Manipulation of the pure spin current can be achieved by controlling the properties of the non-magnetic layer that supports spin current. However, efficient generation, transmission and manipulation of the pure spin current pose great challenges. To efficiently host pure spin currents, the spin relaxation times (τ_s) and spin diffusion lengths (λ_s) are the key parameters which in turn depend on the spin orbit coupling (SOC) of the material. The conventional heavy metal NM layers possess large SOC thus limiting the τ_s and λ_s. In contrast, OSCs consist of low atomic number elements with relatively low SOC strength thereby resulting in higher τ_s and λ_s. Heavy metals which are used as NM in FM/NM spin pumping experiments possess high SOC strength due to their high atomic number and as a result τ_s and λ_s are relatively low. Typically, a FM/NM bilayer structure is used to explore novel phenomena like spin pumping, the spin Hall effect and the inverse spin Hall effect (ISHE) which are associated with the SOC.[10,11] The efficiency of the spin-pumping in a bilayer structure strongly depends on the quality of the interface[12–14] and the SOC of the non-magnetic materials.

To date, several non-magnetic materials, mostly heavy metals such as Ta, Pt, *etc.* are vastly used as NM materials for spin-pumping studies. Recently, inorganic semiconductors such as Si and GaAs have also attracted significant attention for the development of spintronic devices. However, due to the high SOC in these inorganic materials, the spin diffusion lengths and spin relaxation times are small.[15–20] On the other hand, organic semiconductors (OSCs) are an interesting class of materials due to their lightweight, flexibility, cost-effective and solution-processable nature.[21] Because of these superior properties, OSCs are widely explored as active components in

[a]*Department of Materials Science and Metallurgical Engineering, Indian Institute of Technology Hyderabad, Kandi-502285, Telangana, India. E-mail: mchandrasekhar@msme.iith.ac.in*

[b]*Department of Chemistry, Indian Institute of Technology Hyderabad, Kandi-502285, Telangana, India. E-mail: kvrao@chy.iith.ac.in*

[c]*Department of Physics, Indian Institute of Technology Hyderabad, Kandi-502285, Telangana, India*

† Electronic supplementary information (ESI) available. See DOI: 10.1039/d1ra07349d

tunable optoelectronic devices such as organic field-effect transistors (OFETs), organic light-emitting diodes (OLEDs) and solar cells.[22] More recently, OSCs have received significant attention for spintronic device applications owing to their inherently small SOC strength as they are composed of low atomic number (Z) elements such as carbon and hydrogen, potentially making them attractive for carrying the spin currents for longer distances.[23–29] Moreover, the ease of tunability of SOC compared to the inorganic materials makes OSCs potential materials to be used in spin pumping experiments.[30] So far, various conjugated polymers and few small molecules were explored for the spin injection process through ISHE measurements and achieved spin relaxation time and spin diffusion lengths as high as 10 μs and 1.2 μm, respectively.[12,23,28,31–33] Whereas, spin pumping is an effective method for the generation and injection of pure spin current (J_s) at the ferromagnet/non-magnet (FM/NM) interfaces. Pure spin current corresponds to a flow of angular momentum. Tserkovnyak *et al.*[8] have described the spin pumping phenomena in terms of enhancement in Gilbert damping parameter (α) when spins are driven from FM layer to the adjacent NM layer. This enhancement in α is because of the additional magnetization precession due to loss of angular momentum from FM to NM. In spin pumping experiments through FMR technique, the FM layer is driven into precession through microwave excitation and it results in the flow of pure spin current from FM to NM. This reflects in the broadening of absorption spectra which is termed as linewidth broadening. As explained above, it is understood that when there is a spin current injection from FM to its adjacent layer there will be an enhancement in Gilbert damping parameter which will reflect in linewidth broadening of FMR absorption spectra.[31,34,35] So, the measurement of spin injection from a FM material to NM material by using the spin pumping technique and detecting the associated FMR linewidth broadening is considered as one of the direct and precise method for understanding the spin current transparency at the interface between the FM and OSC layers. Recently, Wittmann *et al.* observed FMR linewidth broadening in DNTT based OSCs through spin pumping from permalloy (Py). However, the observed linewidth broadening is relatively small ~0.05 mT.[36] More recently, Vetter *et al.* have used twisted three ploy (3-alkylthiophene) polymers to tune the SOC *via* structural conformation by controlling the conjugation lengths.[30]

In this work, a soft magnetic material $Ni_{80}Fe_{20}$ (permalloy: Py) is chosen as FM acts as the spin source which enable efficient spin injection into the NM layers.[37] We have chosen perylene diimide (PDI) based small molecular OSC as a potential NM material. Among various small molecule based OSCs, PDIs gathered special attention as n-type semiconductors owing to their high chemical and thermal stability, and solution processability.[38,39] Moreover, the optoelectronic properties and supramolecular organization of PDIs can be readily tuned by chemical functionalization at the imide positions and π-conjugated core.[40–43] As a result, PDIs are emerged as an alternative to fullerenes and led to the development of fullerene-free solar cells.[44–46] Moreover, PDIs and their supramolecular materials are widely explored as active components in OFETs, fluorescence spectroscopy, energy storage devices and sensors[47–51] Despite these novel features, to the best of our knowledge, so far PDIs are not explored in spintronic devices. The above-mentioned attractive features may lead to multifunctional devices based on organic semiconductors. This inspired us to use PDIs as novel NM layers in spintronic devices to study the spin pumping from FM materials and uncover its potential in the field of organic spintronics.

Here, we report a giant spin pumping across an interface between a soft FM material, Py and the NM PDI layers. The solution-processable and self-assembling nature of our PDI allowed us to fabricate the NM layer by a simple spin coating method on the substrates. Fig. 1a depicts the stack of PDI/Py, where the M is the magnetization which precess around effective magnetic field (H) and spin current J_s is injected across the interface and σ is the spin polarization vector. In our study, we have directly measured the spin pumping by quantifying the change in FMR linewidth broadening in the FM/NM bilayer in comparison to a bare FM reference layer.[52–54] Notably, we have observed a linewidth change of 2.18 mT, which is more than one order magnitude higher than OSCs reported so far. Moreover, the spin mixing conductance, which governs the spin current injection at the PDI/Py interface, is found to be relatively high *i.e.* 1.54×10^{18} m^{-2} comparable with the spin-mixing conductance of inorganic metals such as Ta and Pt.[15–18]

Experimental methods

To prepare the bilayer structures, a chloroform solution of PDI (0.125 mg mL^{-1}) is spin-coated on pre-cleaned Si substrates under optimized conditions using a spin coater. Next $Ni_{80}Fe_{20}$

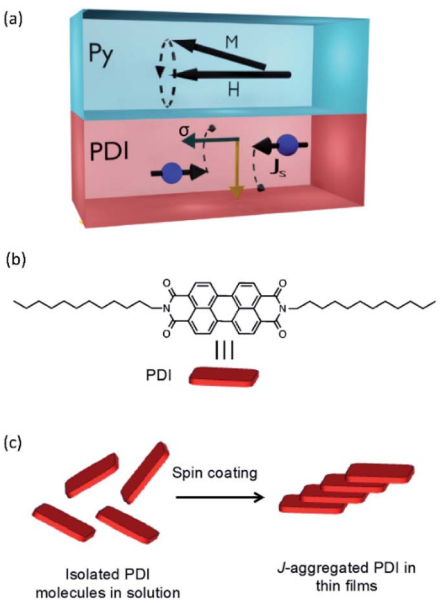

Fig. 1 (a) Schematic illustration of device architecture used for spin pumping experiments under FMR conditions. (b) Molecular structure and schematic representation of PDI. (c) Schematic illustration of the nature of the PDI molecules in a chloroform solution and in the thin film state.

(Py) was sputter-coated on top of PDI using a magnetron sputtering system with a base vacuum better than 3×10^{-7} mbar and the deposition pressure of 5×10^{-3} mbar. To study the spin-pumping we have prepared two sets of samples Si/Py and second Si/PDI/Py. We have made samples with four different thicknesses 4, 8, 12 and 16 nm of Py on Si and Si/PDI. All the Py films are deposited with the same growth parameters and thickness is varied by using deposition time. UV-Visible absorption spectroscopy is used to measure the absorbance spectra of PDI. Atomic force microscopy (AFM) is used to investigate the surface roughness of the Py films deposited on Si and Si/PDI. A lock-in based broadband Ferromagnetic Resonance (FMR) instrument is employed in our work to demonstrate the spin pumping from ferromagnet to nonmagnetic organic semiconductor. The schematic of the setup is as shown in the Fig. 2c. The FMR set-up consists of a RF generator to vary the frequency (4–14 GHz in this study). External magnetic field is generated by an electromagnet with magnetic field ($\mu_0 H$) range of −300 mT to 300 mT which is modulated with a pair of Helmholtz coils attached to the poles of the electromagnet. The frequency (490 Hz) of the external field modulation is used as a reference in the lock-in amplifier for the detection of the FMR signal. RF current is passed through a coplanar waveguide (CPW) and the sample is placed on the CPW in a flip-chip configuration where the sample surface is directly touching the CPW. Due to microwave excitation, FM layer will be driven into precession about the effective magnetic field. At the resonance condition where the RF frequency (h_{rf}) and precession frequency of the magnetization in the sample matches, some amount of RF energy is absorbed by the sample. The energy loss in the RF signal is detected by a RF diode connected to the lock-in amplifier for increasing the signal-to-noise ratio. The resultant signal is a first derivative of absorption intensity with respect to the magnetic field (dI/dH).

Results & discussion

Owing to the solution processable nature of PDI and tendency to form supramolecular assemblies, PDI substituted with dodecyl side chains made to interface with Py. Fig. 1b shows the molecular structure and Fig. 1c depicts J-aggregation of PDI molecules after spin coating. UV-Visible absorption spectroscopy is used since the PDI used in the current study is known to self-assemble in the solid-sate. Shown in Fig. 2a are the UV-Visible spectra which is carried out to probe PDIs molecular organization in the thin film state of PDI. The UV-Visible absorption spectrum of PDI measured in the chloroform (concentration: 0.125 mg mL^{-1}) shows well-resolved vibrational features with a higher intensity of 0–0 peak at 525 nm than 0–1 peak at 488 nm. This is a clear indication of the molecularly soluble state of PDI in chloroform without any aggregation.[55] On the other hand, when taken in dimethyl sulfoxide (DMSO), the 0–0 peak is red-shifted to 570 nm and the spectrum became relatively broad. This indicates the formation of supramolecular assemblies by PDI in DMSO with a slip-stacked arrangement of PDIs (J-aggregation) (Fig. 1c and S1†). These observations are consistent with the previous reports.[56,57]

Interestingly, the absorption spectrum of PDI thin film on Si wafer resembles its absorption spectrum in DMSO (Fig. 2a).[55] It unambiguously proves that PDI self-assemble into J-aggregates when spin-coated from molecularly dissolved chloroform solution on Si wafer. To understand the morphology and roughness of thin film composed of PDI J-aggregates, we have recorded AFM images in the tapping mode which showed the rod-like morphology of PDI J-aggregates and the surface is largely homogeneous without any pinholes. The roughness of bare Py and Py coated on PDI films on Si substrate are found to be below 2 nm (Fig. S2†).

In order to estimate the spin pumping efficiency at the PDI/Py interface, we have recorded the FMR spectra of bilayer PDI/Py structures. We have compared the data with bare Py samples. The derivative FMR data are fitted with asymmetric Lorentzian derivative line shape to extract the linewidth (ΔH) and the resonance field (H_{res}), which is shown in ESI† (Fig. S3). Fig. 3a shows the FMR response of PDI/Py(16) at different frequencies ranging from 4 to 14 GHz. Fig. 3b is the plot of the excitation frequency (f) as a function of H_{res} which is subsequently fitted to the Kittel equation (eqn (1)):

$$f = \frac{\gamma}{2\pi}\sqrt{(H_{res} + H_k + 4\pi M_{eff})(H_{res} + H_k)} \quad (1)$$

where, γ is the gyromagnetic ratio, $4\pi M_{eff}$, H_k represent effective magnetization, magnetic anisotropy field respectively.

On the other hand, the linewidth (ΔH) of the FMR mode (f) is directly related to the damping constant, α as per the following relation:

$$\Delta H = \Delta H_o + \frac{4\pi\alpha_{eff} f}{\gamma} \quad (2)$$

where, ΔH_o denotes an inhomogeneous linewidth broadening that appears due to the inhomogeneity in the ferromagnetic layer. Fig. 3c shows the linewidth *vs.* frequency plot along with a fit to the eqn (2). The linear behaviour of ΔH *vs.* frequency implies good homogeneity in our samples and the relatively low value of the ΔH_o indicates the high quality of the deposited films.

To extract the spin-mixing conductance ($g_{\uparrow\downarrow}$) we have prepared samples (Si/PDI/Py(t) and Si/Py(t)) with varied Py

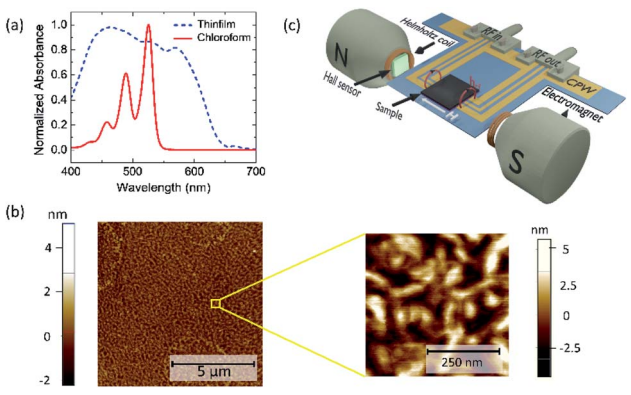

Fig. 2 (a) Normalized UV-Vis absorption spectra of PDI in chloroform (0.125 mg mL^{-1}) and on a Si substrate. (b) AFM image of the spin-coated PDI thin film on a Si substrate (10 μm × 10 μm) and (0.5 μm × 0.5 μm) (c) the schematic illustration of the measurement setup employed in our spin pumping studies.

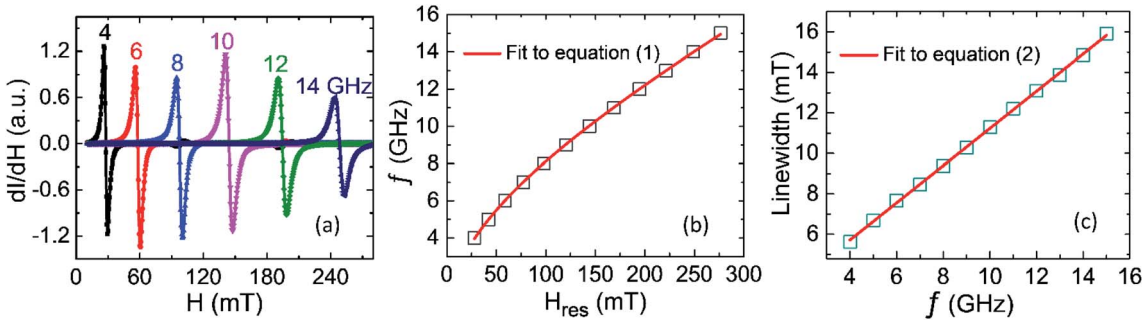

Fig. 3 (a) Derivative FMR responses of PDI/Py(16) for different excitation frequencies. (b) Frequency *vs.* H_{res} plot and Kittel fit for PDI/Py(16). (c) Linewidth *vs.* frequency plot and fit to eqn (2) for PDI/Py(16).

thickness $t = 4$, 8, 12 and 16 nm. Fig. 4a shows the comparison of FMR spectra of Si/PDI/Py(t) and the corresponding reference films *i.e.* Si/Py(t) at the microwave excitation frequency of 9 GHz. The linewidth broadening is observed in all the Py films grown on PDI as compared to the respective reference samples as shown in Fig. 4a–d. The shift in H_{res} is also quite evident in the PDI/Py structures as compared to the reference Py. The shift is higher for lower thickness (4 nm) of Py *i.e.* from 118.2 mT of Py to 123.1 mT of PDI/Py which is reduced as we go towards a higher thickness (16 nm) of Py *i.e.* from 106.3 mT of Py to 108.5 mT of PDI/Py. The shift in the resonance field is due to a change in the effective magnetization of the Py deposited on PDI as compared to the reference Py deposited on Si substrate. The change in effective magnetization between PDI/Py and Py is reduced for 16 nm Py which could be due to diminished influence of the interface due to the thick FM layer in comparison to the case with 4 nm-thick Py sample where the interface effect dominates due to a small thickness of the FM layer. The effective magnetization of the Py layer deposited on PDI as a function of thickness is presented in the ESI† (Fig. S4).

We have plotted the linewidth of the FMR modes of PDI/Py(t) and reference Py(t) films at 9 GHz in Fig. 5. There is a significant increase in the linewidth from reference bare-Py-films to bilayer PDI/Py samples for all the thicknesses of Py. Such a linewidth broadening indicates a strong spin pumping effect *i.e.* a transfer of spin angular momentum from the FM layer to the OSC layer. The transfer of angular momentum at the interface leads to the spin current injection at the interface. The maximum change in linewidth ($\delta\Delta H$) is observed in PDI/Py(16 nm) is 2.18 mT and the minimum $\delta\Delta H$ is observed in PDI/Py(4 nm) is 0.53 mT. This increasing trend in $\delta\Delta H$ from PDI/Py(4 nm) to PDI/Py(16 nm) is observed with the increase in thickness of permalloy, this is because the precession volume will increase with increase in thickness of Py, resulting in injecting more spin currents to the adjacent PDI layer. Recently spin pumping in a Py/DNTT bilayer system is reported using a cavity-based electron spin resonance experiment at 9.4 GHz. Note that a linewidth change of only 0.05 mT is observed in Py/DNTT as compared to a reference bare-Py-layer.[36] In contrast, the linewidth broadening in the present PDI/Py films is quite prominent as compared to the results reported in Py/DNTT.

Furthermore, we have investigated the resonant modes and subsequently extracted the linewidths for a wide range of microwave excitation frequencies (4–14 GHz) and the results are plotted in Fig. 6a–d. The trends are consistent across all the microwave frequencies thereby indicating the uniformity in our samples. According to eqn (2), an increase in the slope of PDI/Py(t) compared to Py(t) in ΔH *vs.* f plots suggests an increase in the damping for PDI/Py(t) in comparison to bare-Py(t) films. The results further confirm the strong spin pumping effect. A shift in H_{res} is observed in PDI/Py(t) compared to their corresponding

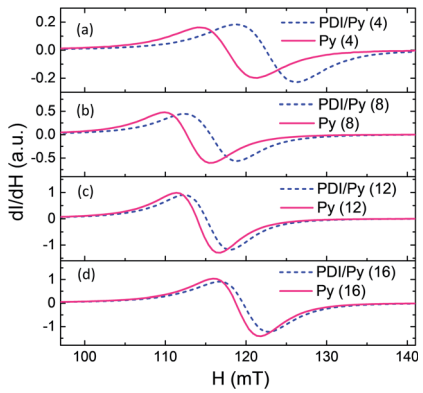

Fig. 4 (a–d) FMR spectra for PDI/Py(t) and reference Py(t) films for $t =$ 4, 8, 12 and 16 nm.

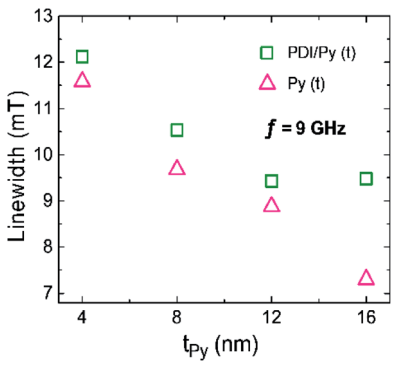

Fig. 5 Linewidth values of PDI/Py and reference Py films for all the thicknesses of Py at $f = 9$ GHz.

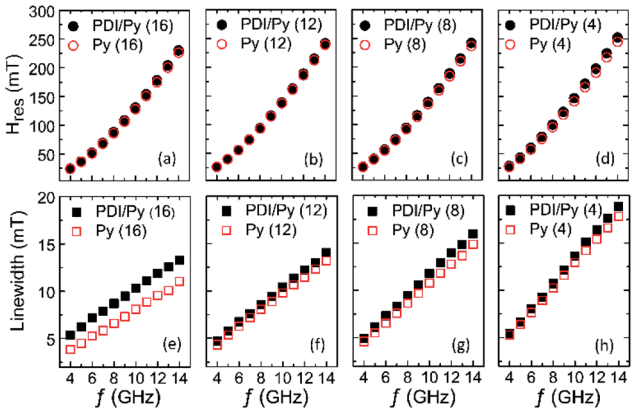

Fig. 6 (a–d) Comparison of resonance field (H_{res}) of PDI/Py(t) and reference Py(t) films for t = 16, 12, 8 and 4 nm. (e–h) Comparison of linewidths of PDI/Py(t) and reference Py(t) films for t = 16, 12, 8 and 4 nm.

Py(t) at all the excitation frequencies (4–14 GHz) as shown in Fig. 6e–h which again reiterates the consistency in our samples.

Quantification of the spin pumping is essential to assess the potential of the OSC (PDI) systems as spin absorbing layers. The efficiency of the spin pumping at the interface can be determined by extracting $g_{\uparrow\downarrow}$ that defines the spin-current transparency at the interface. The $g_{\uparrow\downarrow}$ can be measured by calculating the effective damping parameter (α_{eff})as a function of Py thickness (t_{FM}).[18,54]

The effective damping in bilayer structure is defined as

$$\alpha_{eff} = \alpha_o + \frac{\gamma\hbar g_{\uparrow\downarrow}}{4\pi M_s t_{FM}} \quad (3)$$

where, α_o is the intrinsic damping of the Py layer which is found to be 0.009, $4\pi M_s$ is the saturation magnetization of Py layer which is estimated to be 879.2 mT by fitting to the thickness dependence of $4\pi M_{eff}$ which is shown in the ESI† (Fig. S4). The value of $g_{\uparrow\downarrow}$ is extracted from the slope of the linear fit of α_{eff} *vs.* $1/t_{FM}$ data (shown in Fig. 7) using eqn (3) and it is found to be 1.54×10^{18} m^{-2} which is nearly in the order of conventional FM/heavy metal interface[15–18] and also comparable with Py/DNTT interface.[36] By extracting spin mixing conductance by fitting ferromagnetic layer thickness (t_{FM}) dependence of effective damping parameter, we have eliminated the ambiguity in finding out the effective spin mixing conductance at the interface between Py and PDI.

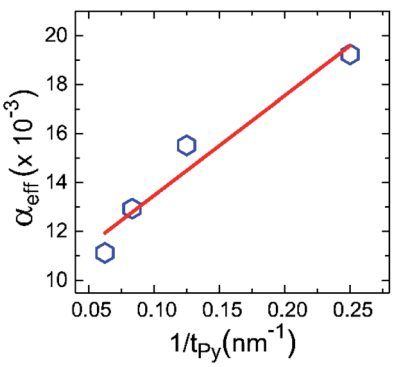

Fig. 7 α_{eff} *vs.* $1/t_{Py}$ plot for PDI/Py(t).

In our work through UV-Vis spectroscopy, we have confirmed that PDI forms J-aggregates upon the spin coating on Si surface. However, the aggregates are short (50–100 nm) in length and randomly oriented on the surface as evident from AFM investigation. Due to this disorder, the SOC of PDI may be relatively higher than expected. From the literature, it is known that the PDIs have comparatively higher charge carrier mobility compared to other organic semiconductors.[51]

A similar observation was made by Vetter *et al.* when they have studied P_3MT and P_3HT for spin current applications. They found that the out-of-plane arrangement of polymer columns in P3MT has resulted in enhancement in the damping parameter and they have observed an increase in SOC due to twisting in the polymer backbone which is because of the increased disorder compared to the ordered lamellar stacks of P_3HT which are horizontally aligned. As a result, P_3MT shows better spin mixing conductance than P_3HT. Li *et al.* has achieved a spin diffusion length of 64 nm at 4.2 K in an n-type semiconductor *i.e.*, P(NDI2OD-T2) and they have attributed long spin diffusion lengths to the high carrier mobility.[58] It is said that the increase in charge carrier mobility prevents scattering during spin transport.[59] The giant spin transport (enhancement of damping, linewidth broadening of 2.18 mT and high spin mixing conductance) from Py to PDI reported in our study was supported by previously mentioned reports. The PDI which is deposited using spin coating has shown a disordered arrangement of J-aggregates and it has inherent higher charge carrier mobility as compared to DNTT,[36] P_3MT and P_3HT4.[30] We believe that the combination of both these factors that are mentioned above may be attributed to the enhancement of spin pumping into PDI from Py. Our results suggest that PDI can be used as non-magnetic layers for spin injection from ferromagnetic layers irrespective of the resistance mismatch.

Conclusions

In summary, we have reported giant spin-pumping across PDI/Py interface where PDI is an OSC with good chemical and thermal stability. FMR linewidth broadening is a direct method to demonstrate and quantify the spin current transparency at the interface between NM and FM. FMR spectra reveal the linewidth broadening of 2.18 mT for PDI/Py(16 nm) at 9 GHz which is more than one order of magnitude higher than any OSCs reported so far. The spin current injected from Py to PDI J-aggregates *via* spin mixing conductance is 1.54×10^{18} m^{-2} which was estimated from thickness dependence of α_{eff} which is in the range of widely explored FM/heavy metal interfaces. Moreover, the solution processable nature, tunable optoelectronic properties and self-assembly behaviour of PDI will open many opportunities to explore this novel class of OSC for spintronic applications. We believe that the results presented here will encourage the study of various OSCs to result in a novel class of organic spintronic devices.

Author contributions

CM – conceptualization, funding acquisition, supervision and writing (review & editing); KVR – conceptualization, resources and writing (review & editing); AH – resources and writing (review & editing); TM – investigation and writing (original draft); SK – investigation and writing (review & editing); BP – investigation and writing (review & editing); SD – investigation.

Conflicts of interest

There are no conflicts to declare.

Acknowledgements

CM would like to acknowledge funding from SERB-Early Career Research Award (ECR/2018/002664). KVR acknowledge SERB-Early Career Research Award (ECR/2018/001222), government of India for the financial support. AH would like to acknowledge funding from Ramanujan Fellowship (SB/S2/RJN-118/2016), Department of science and Technology, India. TM and DS acknowledges the funding from Ministry of Education (MoE) for pursing PhD BP would like to acknowledge fellowship from the Department of science and Technology, India (DST/INSPIRE Fellowship/[IF180927]). SK thanks the CSIR, India for the junior research fellowship. Authors would like to thank Dr Shourya Dutta Gupta and Mr Jayakumar Pillangrovi for facilitating spin coating unit.

Notes and references

1 A. Fert and I. A. Campbell, Two-current conduction in nickel, *Phys. Rev. Lett.*, 1968, **21**, 1190–1192.
2 A. Fert and I. A. Campbell, Electrical resistivity of ferromagnetic nickel and iron based alloys, *J. Phys. F Met. Phys.*, 1976, **6**, 849–871.
3 J. F. Gregg, *Spin Electronics*, Springer, 2001.
4 A. Moser, K. Takano, D. T. Margulies, M. Albrecht, Y. Sonobe, Y. Ikeda, S. Sun and E. E. Fullerton, Magnetic recording: Advancing into the future, *J. Phys. D. Appl. Phys.*, 2002, **35**, R157–R167.
5 N. Nagaosa, Spin currents in semiconductors, metals, and insulators, *J. Phys. Soc. Jpn.*, 2008, **77**, 031010.
6 Y. Kajiwara, K. Harii, S. Takahashi, J. Ohe, K. Uchida, M. Mizuguchi, H. Umezawa, H. Kawai, K. Ando, K. Takanashi, S. Maekawa and E. Saitoh, Transmission of electrical signals by spin-wave interconversion in a magnetic insulator, *Nature*, 2010, **464**, 262–266.
7 I. Žutić, J. Fabian and S. Das Sarma, Spintronics: Fundamentals and applications, *Rev. Mod. Phys.*, 2004, **76**, 323–410.
8 Y. Tserkovnyak, A. Brataas and G. E. W. Bauer, Enhanced Gilbert Damping in Thin Ferromagnetic Films, *Phys. Rev. Lett.*, 2002, **88**, 117601.
9 M. V Costache, M. Sladkov, S. M. Watts, C. H. Van Der Wal and B. J. Van Wees, Electrical Detection of Spin Pumping due to the Precessing Magnetization of a Single Ferromagnet, *Phys. Rev. Lett.*, 2006, **97**, 216603.
10 J. E. Hirsch, Spin Hall Effect, *Phys. Rev. Lett.*, 1999, **83**, 1834.
11 E. Saitoh, M. Ueda, H. Miyajima and G. Tatara, Conversion of spin current into charge current at room temperature: Inverse spin-Hall effect, *Appl. Phys. Lett.*, 2006, **88**, 15–18.
12 T. Li, L. Xu, X. Xiao, F. Chen, L. Cao, W. Wu, W. Tong and F. Zhang, Enhanced Spin Transport of Conjugated Polymer in the Semiconductor/Insulating Polymer Blend, *ACS Appl. Mater. Interfaces*, 2020, **12**, 2708–2716.
13 S. Mallik, A. S. Mohd, A. Koutsioubas, S. Mattauch, B. Satpati, T. Brückel and S. Bedanta, Tuning spinterface properties in iron/fullerene thin films, *Nanotechnology*, 2019, **30**, 435705.
14 T. S. Santos, J. S. Lee, P. Migdal, I. C. Lekshmi, B. Satpati and J. S. Moodera, Room-temperature tunnel magnetoresistance and spin-polarized tunneling through an organic semiconductor barrier, *Phys. Rev. Lett.*, 2007, **98**, 016601.
15 K. Ando, Y. Kajiwara, S. Takahashi, S. Maekawa, K. Takemoto, M. Takatsu and E. Saitoh, Angular dependence of inverse spin-Hall effect induced by spin pumping investigated in a Ni81 Fe19/Pt thin film, *Phys. Rev. B: Condens. Matter Mater. Phys.*, 2008, **78**, 014413.
16 K. Ando, J. Ieda, K. Sasage, S. Takahashi, S. Maekawa and E. Saitoh, Electric detection of spin wave resonance using inverse spin-Hall effect, *Appl. Phys. Lett.*, 2009, **94**, 262505.
17 H. Nakayama, K. Ando, K. Harii, T. Yoshino, R. Takahashi, Y. Kajiwara, K. Uchida, Y. Fujikawa and E. Saitoh, Geometry dependence on inverse spin Hall effect induced by spin pumping in Ni 81Fe 19/Pt films, *Phys. Rev. B: Condens. Matter Mater. Phys.*, 2012, **85**, 144408.
18 A. Kumar, R. Bansal, S. Chaudhary and P. K. Muduli, Large spin current generation by the spin Hall effect in mixed crystalline phase Ta thin films, *Phys. Rev. B*, 2018, **98**, 104403.
19 I. Appelbaum, B. Huang and D. J. Monsma, Electronic measurement and control of spin transport in silicon, *Nature*, 2007, **447**, 295–298.
20 J. M. Kikkawa and D. D. Awschalom, Lateral drag of spin coherence in gallium arsenide, *Nature*, 1999, **397**, 139–141.
21 T. F. A. De Greef, M. M. J. Smulders, M. Wolffs, A. P. H. J. Schenning, R. P. Sijbesma and E. W. Meijer, Supramolecular polymerization, *Chem. Rev.*, 2009, **109**, 5687–5754.
22 L. Brunsveld, B. J. B. Folmer, E. W. Meijer and R. P. Sijbesma, Supramolecular polymers, *Chem. Rev.*, 2001, **101**(12), 4071–4097.
23 V. Dediu, M. Murgia, F. C. Matacotta, C. Taliani and S. Barbanera, Room temperature spin polarized injection in organic semiconductor, *Solid State Commun.*, 2002, **122**, 181–1844.
24 V. A. Dediu, L. E. Hueso, I. Bergenti and C. Taliani, Spin routes in organic semiconductors, *Nat. Mater.*, 2009, **8**, 707–716.
25 G. Szulczewski, S. Sanvito and M. Coey, A spin of their own, *Nat. Mater.*, 2009, **8**, 693–695.

26 J. Yakhmi and V. Bambole, Molecular spintronics, *Solid State Phenom.*, 2012, **189**, 95–127.
27 Y. Zheng and F. Wudl, Organic spin transporting materials: Present and future, *J. Mater. Chem. A*, 2014, **2**, 48–57.
28 S. J. Wang, D. Venkateshvaran, M. R. Mahani, U. Chopra, E. R. McNellis, R. Di Pietro, S. Schott, A. Wittmann, G. Schweicher, M. Cubukcu, K. Kang, R. Carey, T. J. Wagner, J. N. M. Siebrecht, D. P. G. H. Wong, I. E. Jacobs, R. O. Aboljadayel, A. Ionescu, S. A. Egorov, S. Mueller, O. Zadvorna, P. Skalski, C. Jellett, M. Little, A. Marks, I. McCulloch, J. Wunderlich, J. Sinova and H. Sirringhaus, Long spin diffusion lengths in doped conjugated polymers due to enhanced exchange coupling, *Nat. Electron.*, 2019, **2**, 98–107.
29 L. Guo, Y. Qin, X. Gu, X. Zhu, Q. Zhou and X. Sun, Spin transport in organic molecules, *Front. Chem.*, 2019, **7**, 428.
30 E. Vetter, I. VonWald, S. Yang, L. Yan, S. Koohfar, D. Kumah, Z.-G. Yu, W. You and D. Sun, Tuning of spin-orbit coupling in metal-free conjugated polymers by structural conformation, *Phys. Rev. Mater.*, 2020, **4**, 085603.
31 D. Sun, K. J. Van Schooten, M. Kavand, H. Malissa, C. Zhang, M. Groesbeck, C. Boehme and Z. Valy Vardeny, Inverse spin Hall effect from pulsed spin current in organic semiconductors with tunable spin-orbit coupling, *Nat. Mater.*, 2016, **15**, 863–869.
32 S. Watanabe, K. Ando, K. Kang, S. Mooser, Y. Vaynzof, H. Kurebayashi, E. Saitoh and H. Sirringhaus, Polaron spin current transport in organic semiconductors, *Nat. Phys.*, 2014, **10**, 308–313.
33 X. Sun, A. Bedoya-Pinto, Z. Mao, M. Gobbi, W. Yan, Y. Guo, A. Atxabal, R. Llopis, G. Yu, Y. Liu, A. Chuvilin, F. Casanova and L. E. Hueso, Active Morphology Control for Concomitant Long Distance Spin Transport and Photoresponse in a Single Organic Device, *Adv. Mater.*, 2016, **28**, 2609–2615.
34 S. Mizukami, Y. Ando and T. Miyazaki, The study on ferromagnetic resonance linewidth for NM/80NiFe/NM (NM = Cu, Ta, Pd and Pt) films, *Jpn. J. Appl. Phys., Part 1*, 2001, **40**, 580–585.
35 M. Haertinger, C. H. Back, J. Lotze, M. Weiler, S. Geprägs, H. Huebl, S. T. B. Goennenwein and G. Woltersdorf, Spin pumping in YIG/Pt bilayers as a function of layer thickness, *Phys. Rev. B: Condens. Matter Mater. Phys.*, 2015, **92**, 1–6.
36 A. Wittmann, G. Schweicher, K. Broch, J. Novak, V. Lami, D. Cornil, E. R. McNellis, O. Zadvorna, D. Venkateshvaran, K. Takimiya, Y. H. Geerts, J. Cornil, Y. Vaynzof, J. Sinova, S. Watanabe and H. Sirringhaus, Tuning Spin Current Injection at Ferromagnet-Nonmagnet Interfaces by Molecular Design, *Phys. Rev. Lett.*, 2020, **124**, 027204.
37 K. Ando, T. Yoshino and E. Saitoh, Optimum condition for spin-current generation from magnetization precession in thin film systems, *Appl. Phys. Lett.*, 2009, **94**, 152509.
38 F. Würthner, C. R. Saha-Möller, B. Fimmel, S. Ogi, P. Leowanawat and D. Schmidt, Perylene Bisimide Dye Assemblies as Archetype Functional Supramolecular Materials, *Chem. Rev.*, 2016, **116**, 962–1052.
39 F. Zhang, Y. Ma, Y. Chi, H. Yu, Y. Li, T. Jiang, X. Wei and J. Shi, Self-assembly, optical and electrical properties of perylene diimide dyes bearing unsymmetrical substituents at bay position, *Sci. Rep.*, 2018, **8**, 8208.
40 F. Nolde, W. Pisula, S. Müller, C. Kohl and K. Müllen, Synthesis and self-organization of core-extended perylene tetracarboxdiimides with branched alkyl substituents, *Chem. Mater.*, 2006, **18**, 3715–3725.
41 A. Wicklein, A. Lang, M. Muth and M. Thelakkat, Swallow-tail substituted liquid crystalline perylene bisimides: Synthesis and thermotropic properties, *J. Am. Chem. Soc.*, 2009, **131**, 14442–14453.
42 F. Würthner, B. Hanke, M. Lysetska, G. Lambright and G. S. Harms, Gelation of a highly fluorescent urea-functionalized perylene bisimide dye, *Org. Lett.*, 2005, **7**, 967–970.
43 S. Kotha, M. F. J. Mabesoone, D. Srideep, R. Sahu, S. K. Reddy and K. V. Rao, Supramolecular Depolymerization in the Mixture of Two Poor Solvents: Mechanistic Insights and Modulation of Supramolecular Polymerization of Ionic π-Systems, *Angew. Chem., Int. Ed.*, 2021, **60**, 5459–5466.
44 P. K. Sukul, A. Datta and S. Malik, Light harvesting and amplification of emission of donor perylene-acceptor perylene aggregates in aqueous medium, *Chem. – Eur. J.*, 2014, **20**, 3019–3022.
45 W. Chen and Q. Zhang, Recent progress in non-fullerene small molecule acceptors in organic solar cells (OSCs), *J. Mater. Chem. C*, 2017, **5**, 1275–1302.
46 D. M. Stoltzfus, J. E. Donaghey, A. Armin, P. E. Shaw, P. L. Burn and P. Meredith, Charge Generation Pathways in Organic Solar Cells: Assessing the Contribution from the Electron Acceptor, *Chem. Rev.*, 2016, **116**, 12920–12955.
47 T. B. Schon, A. J. Tilley, E. L. Kynaston and D. S. Seferos, Three-Dimensional Arylene Diimide Frameworks for Highly Stable Lithium Ion Batteries, *ACS Appl. Mater. Interfaces*, 2017, **9**(18), 15631–15637.
48 P. Gawrys, D. Boudinet, M. Zagorska, D. Djurado, J. M. Verilhac, G. Horowitz, J. Pécaud, S. Pouget and A. Pron, Solution processible naphthalene and perylene bisimides: Synthesis, electrochemical characterization and application to organic field effect transistors (OFETs) fabrication, *Synth. Met.*, 2009, **159**, 1478–1485.
49 M. Madhu, R. Ramakrishnan, V. Vijay and M. Hariharan, Free Charge Carriers in Homo-Sorted π-Stacks of Donor–Acceptor Conjugates, *Chem. Rev.*, 2021, **121**(13), 8234–8284.
50 P. Ranque, C. George, R. K. Dubey, R. Van Der Jagt, D. Flahaut, R. Dedryvère, M. Fehse, P. Kassanos, W. F. Jager, E. J. R. Sudhölter and E. M. Kelder, Scalable Route to Electroactive and Light Active Perylene Diimide Dye Polymer Binder for Lithium-Ion Batteries, *ACS Appl. Energy Mater.*, 2020, **3**, 2271–2277.
51 F. May, V. Marcon, M. R. Hansen, F. Grozema and D. Andrienko, Relationship between supramolecular assembly and charge-carrier mobility in perylenediimide derivatives: The impact of side chains, *J. Mater. Chem.*, 2011, **21**, 9538–9545.

52 J. M. Shaw, H. T. Nembach and T. J. Silva, Determination of spin pumping as a source of linewidth in sputtered Co 90Fe 10/Pd multilayers by use of broadband ferromagnetic resonance spectroscopy, *Phys. Rev. B: Condens. Matter Mater. Phys.*, 2012, **85**, 054412.

53 H. Wang, A. Pomar, S. Martín-Rio, C. Frontera, N. Mestres and B. Martínez, Dynamic magnetic properties and spin pumping in polymer-assisted-deposited La0.92MnO3 thin films, *J. Mater. Chem. C*, 2019, **7**, 12633–12640.

54 R. Bansal, A. Kumar, N. Chowdhury, N. Sisodia, A. Barvat, A. Dogra, P. Pal and P. K. Muduli, Extrinsic spin-orbit coupling induced enhanced spin pumping in few-layer MoS 2/Py, *J. Magn. Magn. Mater.*, 2019, **4**, 337.

55 K. Balakrishnan, A. Datar, T. Naddo, J. Huang, R. Oitker, M. Yen, J. Zhao and L. Zang, Effect of side-chain substituents on self-assembly of perylene diimide molecules: Morphology control, *J. Am. Chem. Soc.*, 2006, **128**, 7390–7398.

56 Z. Chen, B. Fimmel and F. Würthner, Solvent and substituent effects on aggregation constants of perylene bisimide π-stacks - A linear free energy relationship analysis, *Org. Biomol. Chem.*, 2012, **10**, 5845–5855.

57 E. H. A. Beckers, S. C. J. Meskers, A. P. H. J. Schenning, Z. Chen, F. Würthner, P. Marsal, D. Beljonne, J. Cornil and R. A. J. Janssen, Influence of intermolecular orientation on the photoinduced charge transfer kinetics in self-assembled aggregates of donor-acceptor arrays, *J. Am. Chem. Soc.*, 2006, **128**, 649–657.

58 F. Li, T. Li, F. Chen and F. Zhang, Excellent spin transport in spin valves based on the conjugated polymer with high carrier mobility, *Sci. Rep.*, 2015, **5**, 9355.

59 L. Guo, Y. Qin, X. Gu, X. Zhu, Q. Zhou and X. Sun, Spin transport in organic molecules, *Front. Chem.*, 2019, **7**, 428.